



Compressor speed control for optimizing energy matching of PV-driven AC systems during the cooling season

Kai Wang^a, Jinqing Peng^{a,b,*}, Sihui Li^c, Houpei Li^{a,b}, Bin Zou^{a,b}, Tao Ma^d, Jie Ji^e

^a College of Civil Engineering, Hunan University, Changsha, Hunan, China

^b Key Laboratory of Building Safety and Energy Efficiency of Ministry of Education, Hunan University, Changsha, Hunan, China

^c College of Energy and Power Engineering, Changsha University of Science and Technology, Changsha, Hunan, China

^d School of Mechanical Engineering, Shanghai Jiao Tong University, Shanghai, China

^e Department of Thermal Science and Energy Engineering, University of Science and Technology of China, Hefei, Anhui, China

ARTICLE INFO

Keywords:

Photovoltaic driven air conditioning systems

(PVAC)

Compressor speed control

Air conditioning load flexibility

Energy matching

ABSTRACT

Photovoltaic-driven air conditioning (PVAC) systems innovatively utilize PV power for building cooling, reducing PV power fluctuation impact on the utility grid. This study introduced a novel PVAC system that optimizes the energy matching between PV generation and air conditioning electricity demand through directly controlling of the compressor speed in accordance with the real-time PV power generation. A PID control method was employed to regulate the compressor speed of PVAC, and three control strategies were proposed and successfully implemented during the experiments. The system's efficiency was evaluated using metrics such as the self-consumption rate (SCR), self-sufficiency rate (SSR), real-time zero energy proportion (RZEP), and the mean absolute error (MAE) of indoor temperature. The results of this study confirm that the proposed control method significantly enhances the power matching between the PV power generation and the air conditioning electricity demand. Implementing the recommended strategy, SCR increased from 0.53 to 0.625 and SSR from 0.716 to 0.808, all while maintaining indoor thermal comfort. Moreover, the proposed approach mitigates the impact of distributed PV generation on the utility grid and potentially diminishes energy storage needs, which can contribute to a lower system investment requirements and operating costs.

1. Introduction

The global energy crisis is one of the foremost challenges currently faced by the world [1]. With the rapid growth of electricity demand in China and other countries [2], it has become crucial to explore alternative energy sources and methods for efficient utilization of existing energy resources. Renewable energy, particularly wind energy and solar photovoltaic (PV) energy, are widely considered as a promising solution to handle this energy crisis [1]. However, renewable energy generation faces challenges such as intermittency, variability, and uncertainty, leading to considerable fluctuations in power output [3]. These fluctuations pose a threat to the operational stability of the public utility grid [4].

In China, the building sector accounts for a significant proportion of national energy consumption and carbon emissions, with air conditioning units being a major energy consumer within buildings [5,6]. The integration of distributed PV with buildings traditionally entails a direct

connection of PV generation to the utility grid, placing a dual burden on the grid and leading to voltage instability and complexities in microgrid balancing [7]. As the penetration rate of distributed PV increasing, traditional energy generation resources struggle to respond to abrupt changes of PV generation and net electricity demand, often resulting in the curtailment of PV power generation [8,9]. Therefore, the real-time integration of PV power generation on the demand side requires consideration.

There is a correlation between PV power generation and building air conditioning demand [10], with periods of high PV generation often coinciding with increased cooling demand from air conditioning due to their shared dependence on solar radiation intensity. This presents an opportunity to utilize PV power generation to directly drive air conditioning (AC) systems. The PV-driven air conditioning (PVAC) system integrates a vapor compression refrigeration system with a PV power generation system, enabling on-site utilization of PV power [11]. Previous studies have extensively investigated this topic [12,13]. For

* Corresponding author. College of Civil Engineering, Hunan University, Changsha, 410082, Hunan, China.

E-mail address: jqpeng@hnu.edu.cn (J. Peng).

<https://doi.org/10.1016/j.energy.2024.131270>

Received 23 October 2023; Received in revised form 22 February 2024; Accepted 8 April 2024

Available online 13 April 2024

0360-5442/© 2024 Elsevier Ltd. All rights reserved.

instance, Liang et al. [14] explored the economic impact of various types of cold-thermal energy storage (CTES) on PVAC systems in tropical regions, concluding that batteries, despite their expensive cost [15], are indispensable in off-grid PVAC systems, while other storage forms can partially replace batteries and reduce system costs. A more suitable approach for building air conditioning systems is a grid-connected PVAC system [16,17], which prioritizes meeting the energy demands of air conditioning units using PV generation, and supplies surplus energy if any to the utility grid. This approach effectively reduces the impact of PV generation on the utility grid and the net energy demand from the utility grid. However, due to the thermal inertia of buildings, the building cooling load does not fluctuate as rapidly as PV generation, which can affect the matching between PV generation and building cooling demand [16].

Various strategies can be used to enhance the energy matching of PVAC systems. Li et al. [18] considered the use of phase change materials (PCM) and building load flexibility to improve the real-time zero-energy probability (RZEP) of PVAC systems during the system design stage. The majority of research focused on control optimization during system operation, as it required minimal modification to the existing buildings and systems [19]. Gao et al. [20,21] proposed a variable compressor speed PV direct current cooling system and found that the maximum power point tracking (MPPT) method was currently the best control method to improve the cooling capacity of the system. Notably, due to the flexibility of building loads [22], a wide range of regulation exists for air conditioning system control [16]. Schibuola et al. [23] proposed three control strategies based on dynamic electricity prices and PV generation for on/off control HVAC systems. Zhao et al. [24] presented an adaptive PID control method that enhances the matching between PV generation and air conditioning load by adjusting the air conditioner temperature setpoint without sacrificing indoor thermal comfort. Li et al. [25] proposed an off-grid PVAC system with ice storage cooling. Their study showed that the system with MPPT controller and variable speed compressor performed optimally. Li et al. [26] developed a coupled simulation model that includes an air conditioning system to evaluate the energy matching characteristics, air conditioning performance, and load flexibility of PVAC systems. Jiang et al. [19] introduced a method that leverages building loads to stabilize the fluctuations of PV power generation. This approach effectively decreased the net energy demand on utility grid. Salpakari et al. [27] considered the impact of energy storage on Heating, Ventilation, and Air Conditioning (HVAC) systems and PV systems and conducted cost-optimal optimization control and rule-based control based on PV integration to reduce operating costs and utility grid power exchange. More complex control methods such as Model Predictive Control (MPC), were also commonly adopted in the control of systems that combine PV system and air conditioning units [28–30], but as they require accurate models, which can be challenging in practice [31].

The existing literature indicates a breadth of research on PVAC system design and operational optimization. This spans areas such as PV cooling system design, energy storage capacity optimization, and refining operational control. Nevertheless, most of these studies primarily focus on improving system performance to enhance cooling capacity, often neglecting the system's interaction with the utility grid. The majority of PVAC control mechanisms rely on on/off control or temperature setpoint adjustments, along with optimizing control algorithms. However, the implementation of complex control methods remains challenging, and the attainment of energy demand-supply balance in smaller time scales still proves to be elusive. As the penetration rate of distributed PV continues to increase, rapid response on the demand side becomes necessary [32]. Directly controlling the compressor speed of the air conditioner to achieve fast tracking and response of the PV power generation is a feasible solution.

This study aims to establish a grid-connected PVAC system, including an experimental platform and a simulation model. This study aims to establish a grid-connected PVAC system, including an experimental

platform and a simulation model. We propose an approach that directly controls the compressor speed of the air conditioner based on the real-time PV power generation using a PID control method. This method allows for dynamic adjustment of the air conditioning system's power consumption to match the fluctuating PV power, thereby enhancing the energy matching performance of the PVAC system. Three control strategies for the proposed PVAC system were presented, and their feasibility was validated through experiments. The experiments analyzed the power tracking performance of the PVAC system and its impact on the utility grid power and voltage. The model was used to analyze the system performance and the influence of energy storage capacity throughout the cooling season. The results indicated that the proposed control methods and strategies can enhance energy matching and reduce the required energy storage capacity of the PVAC system without significantly affecting the indoor thermal environment.

The structure of this paper is as follows: Section 2 describes the PVAC system, including the models of the major components and the evaluation metrics for the system. Section 3 provides the detailed explanations of the methods, including the power control methods and the proposed control strategies. Section 4 describes the experimental setup and presents the validation and feasibility analysis of the control strategies. Section 5 discusses the system performance. Section 6 concludes the main contributions of the study and proposes directions for future research.

2. PVAC system and model description

2.1. PVAC system description

A typical grid-connected PVAC system is shown in Fig. 1. The PV panels transform incident solar energy into electrical energy. This energy, after conversion by the DC/AC inverter, primarily powers the air conditioner. The inverter can connect to both the utility grid and a battery. Notably, electricity flows bi-directionally, both between the utility grid and the inverter and between the battery and the inverter. The PV-generated electricity takes precedence in powering the air conditioner. When there's an electricity shortfall, it's compensated by either the grid or the batteries. On the other hand, excess PV power is directed to either storage in the battery or supply to the grid. In this study, batteries function in a self-generation and self-consumption mode. This means they prioritize compensating for any discrepancies between PV power generation and air conditioning power consumption. Then, a physical PVAC system was built, which is described in detail in Section 4.

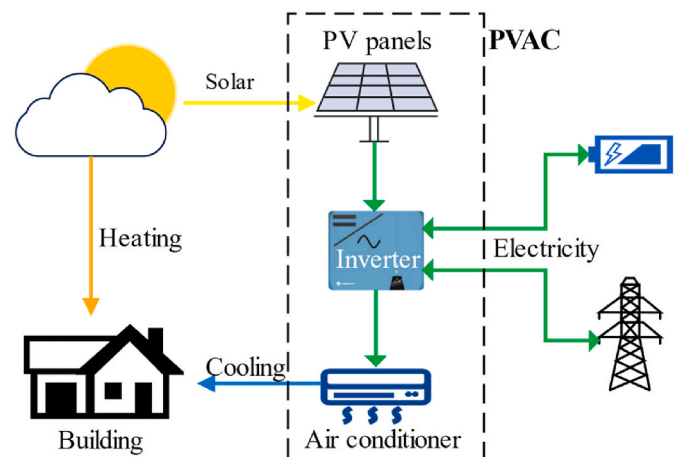


Fig. 1. A typical grid-connected PVAC system.

2.2. PVAC modelling

The energy balance of a PVAC system involves both electrical power balance and thermal power balance. The PV array transforms incident solar radiation into electrical energy that directly powers the air conditioning system. When there is a mismatch between PV generation and air conditioning power consumption, the utility grid or battery steps in to ensure a power balance. The power balance can be described by Eq. (1):

$$P_{PV} + P_{Grid} = P_{AC} + P_{battery} \quad (1)$$

In Equation (1), P_{PV} represents the PV generation power, which is mainly influenced by fluctuating solar radiation and other environmental conditions. P_{Grid} represents the utility grid power, which takes a positive value when drawing power from the utility grid and a negative value when power is fed back into the utility grid. P_{AC} represents the power consumption of the air conditioning system. $P_{battery}$ represents the power charge/discharge of the battery, taking a positive value during charging and a negative value during discharging.

The air conditioning system transitions electrical energy into cooling capacity, influencing the indoor thermal environment. The indoor temperature is influenced by the heat transfer from the building envelope, the cooling capacity of the air conditioning system and the internal heat gain. The thermal balance within the room can be described by Eq. (2):

$$C_r \frac{dT_r}{dt} = Q_{cooling} + Q_{AC} + Q_{ig} \quad (2)$$

In Equation (2), C_r represents the overall thermal capacity of the room. T_r represents the room temperature. $Q_{cooling}$ represents the heat transfer through the building envelope. Q_{AC} represents the cooling capacity of the air conditioning system, with a negative value in the equation. Q_{ig} represents the internal heat gains of the room.

To simulate the operational state of the physical system, models for each component are established in Python as described below.

2.2.1. PV model

The solar radiation incident on the plane of the PV array G_T , is composed of three components, viz: direct radiation G_b , diffuse radiation G_d , and reflected radiation G_r , as shown in Eq. (3) [33]:

$$G_T = G_b + G_d + G_r \quad (3)$$

Detailed calculation methods of G_T can be found in Ref. [34]. With the measured solar radiation and ambient temperature, the power output of the PV system under these conditions can be calculated using Eq. (4):

$$P_{PV} = G_T \times \eta_{cell} \times \eta \times A_{cell} \quad (4)$$

In Equation (4), η represents the PV system's performance ratio, η_{cell} represents the energy conversion efficiency of the PV module under actual operating conditions, and A_{cell} represents the total area of the solar cells within the PV system. Notably, we determined cell temperatures using the Nominal Operating Cell Temperature (NOCT) model. Subsequently, these temperatures were employed to correct η_{cell} , following the methodology described in Ref. [34].

2.2.2. Air conditioning model

Air conditioning systems enable the conversion from electrical to thermal energy in PVAC systems. In this study, we controlled the air conditioning power by modulating the compressor speed. Therefore, it is necessary to establish the relationship among the air conditioning cooling capacity, power consumption, and compressor speed. The air conditioning cooling capacity can be expressed by Eq. (5):

$$Q_{AC} = P_{AC} \times k_{EER} \quad (5)$$

In Equation (5), k_{EER} represents the Energy Efficiency Ratio (EER) of

the air conditioning system during operation. It is mainly influenced by the indoor temperature and the outdoor ambient temperature [35]. In this study, it was simplified and expressed as Eq. (6) [36]:

$$k_{EER} = a_1 + b_1 \times T_o + b_2 \times T_o^2 + c_1 \times T_r + c_2 \times T_r^2 \quad (6)$$

In Equation (6), T_o represents the outdoor ambient temperature, and a_1, b_1, b_2, c_1 and c_2 are constants obtained by fitting the performance curve provided by the manufacturer [37].

In addition, the power consumption of the air conditioning system is mainly influenced by factors such as compressor speed, outdoor ambient temperature, and indoor temperature [38]. To accurately model this relationship, we fitted the power consumption using the measured operating data from our experimental setup. The resulting empirical model is expressed by Eq. (7):

$$\begin{cases} P_{AC} = a_2 + b_3 \times T_o + c_3 \times T_r + d_1 \times N, N \neq 0 \\ P_{AC} = 0, N = 0 \end{cases} \quad (7)$$

In Equation (7), N represents the compressor speed, expressed in revolutions per minute (rpm), and a_2, b_3, c_3 , and d_1 are constants.

2.2.3. Building thermal model

Changes of the outdoor environmental conditions and the operating state of the air conditioning system affect the indoor environment. We adapted a second-order RC thermal network from existing literature [39] to model indoor environment fluctuations. The room was modeled as a box with six opaque surfaces: four walls, a roof, and a floor. Three assumptions were made: 1) The air supplied from the air conditioning system is well mixed, resulting in a uniform indoor temperature distribution. 2) Each wall surface has its own thermal capacity and temperature, and they do not affect each other. This means that each wall surface is only influenced by the indoor and outdoor environments. 3) The thermal capacity of windows is not considered, but the effect of solar radiation on the indoor temperature through the windows is considered. Thus, a building RC model with seven thermal capacitances was established, as shown in Fig. 2.

In Fig. 2, $C_{w,i}$ represents the thermal capacitance of the i -th wall surface. In the actual case study of this research, there are six wall surfaces and two windows: one west-facing window and one south-facing window. For the walls, $T_{w,i}$ indicates the temperature of the i -th wall, and $R_{w,i}$ and $R_{wc,i}$ represent the conductive heat transfer resistance and convective heat transfer resistance of the walls, respectively.

Regarding windows, we opted not to consider their thermal capacitance and temperature, given their limited influence on the overarching thermal dynamics. $R_{w,j}$ and $R_{c,j}$ represent the resistance and convective heat transfer resistance of the j -th window surface, respectively.

When evaluating solar radiation's influence on the building environment, we explored four distinct facets. First, we considered the portion of solar radiation that directly affects the indoor environment after passing through the transparent enclosure. Second, we examined the solar radiation that penetrates the transparent enclosure and impacts

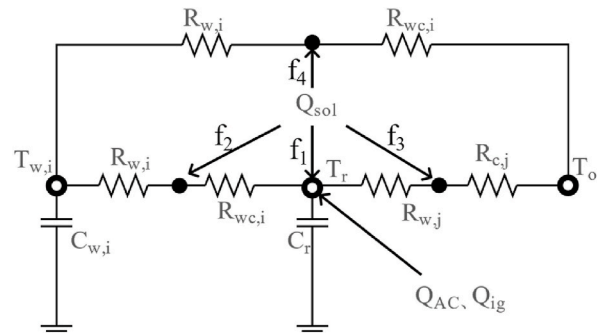


Fig. 2. Schematic diagram of the air-conditioned room RC model.

the walls. Of this radiation, a certain amount is absorbed by the walls, while the remaining portion affects the indoor environment through convective heat transfer. Third, we looked at the solar radiation that interacts with the windows and subsequently influences the indoor environment via convective heat transfer. In our study, we treated the cavity as a blackbody, considering only the solar radiation that entered the room through the window from the outside. Lastly, our attention was drawn to the solar radiation that acts on the outer side of the walls and subsequently permeates through them. Four coefficients, f_1 , f_2 , f_3 and f_4 , indicate the proportion of the energy received by the building from solar radiation, corresponding to the influences of the four components described in the previous sentence. Having defined the invariant thermal parameters according to the actual materials used in the walls and windows of the experimental room, and after verifying them with experimental data, the expressions of the RC model was presented in Eq. (8) and Eq. (9).

$$C_r \frac{dT_r}{dt} = \sum \frac{T_{w,i} - T_r}{R_{w,i} + R_{w,c,i}} + \sum \frac{T_o - T_r}{R_{w,j} + R_{c,j}} + \sum f_1 \times Q_j + \sum f_2 \times Q_{i,j} \times \frac{R_{w,i}}{R_{w,i} + R_{w,c,i}} + \sum f_3 \times Q_j \times \frac{R_{c,j}}{R_{w,j} + R_{c,j}} + Q_{ig} + Q_{AC} \quad (8)$$

$$C_{w,i} \frac{dT_{w,i}}{dt} = \frac{T_r - T_{w,i}}{R_{w,i} + R_{w,c,i}} + \frac{T_o - T_{w,i}}{R_{w,i} + R_{w,c,i}} + f_2 \times Q_{i,j} \times \frac{R_{w,c,i}}{R_{w,i} + R_{w,c,i}} + f_4 \times Q_i \times \frac{R_{w,c,i}}{R_{w,i} + R_{w,c,i}} \quad (9)$$

In Equations (8) and (9), Q_i represents the total solar radiation acting on the surface of the i -th wall, Q_j represents the total solar radiation acting on the surface of the j -th window, and $Q_{i,j}$ represents the total solar radiation reaching the i -th wall after passing through the j -th window.

2.3. PVAC performance indicators

The self-consumption rate (SCR) and self-sufficiency rate (SSR) are commonly used metrics to evaluate the performance of PV systems. For the PVAC system in this study, SCR represents the percentage of electricity generated by the PV system that is consumed by the air conditioning, while SSR represents the ratio of electricity consumed by the air conditioning that comes from PV generation. Eq. (10) and Eq. (11) show the formulations of SCR and SSR, respectively.

$$SCR = \frac{\int_t^{t+1} M(t) dt}{\int_t^{t+1} P_{PV}(t) dt} \quad (10)$$

$$SSR = \frac{\int_t^{t+1} M(t) dt}{\int_t^{t+1} P_{AC}(t) dt} \quad (11)$$

In Equations (10) and (11), $M(t)$ represents the smaller value between real-time PV generation power ($P_{PV}(t)$) and the air conditioning power consumption ($P_{AC}(t)$). It indicates the portion of PV generation directly used by the air conditioning.

Additionally, Li et al. [16] defined the real-time zero energy proportion (RZEP) of PVAC systems as the ratio of the total time with zero energy consumption to the total operating time. It is used to evaluate the energy matching performance of the PVAC system. Eq. (12) presents the calculation of RZEP:

$$RZEP = \frac{\int \kappa(t) dt}{t_{PVAC}} \quad (12)$$

In Equation (12), t_{PVAC} represents the total operating time of the PVAC system, and $\kappa(t)$ is a binary value where 1 indicates that the PV-generated energy can meet the total consumption of the air conditioning system, and 0 indicates that it cannot.

Apart from considering the energy matching performance of the

system, the thermal comfort of the air-conditioned room is an important metric. In this study, the Mean Absolute Error (MAE) between the room temperature T_r and the set temperature (T_{set}) was used to evaluate the effectiveness of the indoor temperature control. Eq. (13) represents the calculation of MAE:

$$MAE = \frac{\int |T_r - T_{set}| dt}{t_{PVAC}} \quad (13)$$

Crucially, the metrics mentioned above are tailored to the PVAC system. SCR and SSR are defined for a certain research period (several days or months), while RZEP and MAE are considered during the operating time of the PVAC system and are not calculated during non-operating periods.

3. Methodology

3.1. Power control method of the PVAC system

To enhance the power matching performance of PVAC systems, this study proposed a control method that directly modulates the compressor speed of the air conditioner, aligning its power consumption with PV power generation. The control principle is illustrated in Fig. 3. When changing the air conditioning operating state, two factors need to be considered. First, the energy matching performance of the system, which refers to the power matching between the PV power generation and the air conditioning consumption. Second but more important, the requirement for maintaining thermal comfort in the indoor environment.

In Fig. 3, there are two control loops. The first one is the power tracking control loop, which takes the real-time PV generation power ($P_{PV}(t)$) as an input. Within the allowable range of compressor speed, the control loop calculates the compressor speed gain based on the difference between the real-time PV generation power ($P_{PV}(t)$) and the real-time air conditioning power consumption ($P_{AC}(t)$), using a PID controller. The PID controller is configured with the following parameters determined through field tuning: (1) Proportional band (P_B): This parameter defines the range over which the proportional action occurs. A smaller P_B value results in a more aggressive response; (2) Integral time (T_I): This parameter integrates the error over time, allowing the controller to eliminate steady-state errors; (3) Differential time (T_D): This parameter predicts the future behavior of the error, providing a damping effect to the control action. The tuning process involved adjusting P_B , T_I , and T_D values to achieve a balance between responsiveness and stability, ensuring optimal power tracking and minimizing fluctuations in the system's performance.

The calculated gain is then sent as an instruction to the compressor speed controller, which adjusts the air conditioning operation accordingly. Following the adjustment of the air conditioning operation, the real-time compressor speed ($N(t)$) and $P_{AC}(t)$ are obtained and relayed back to the controller.

The second control loop is the temperature control, which adjusts the

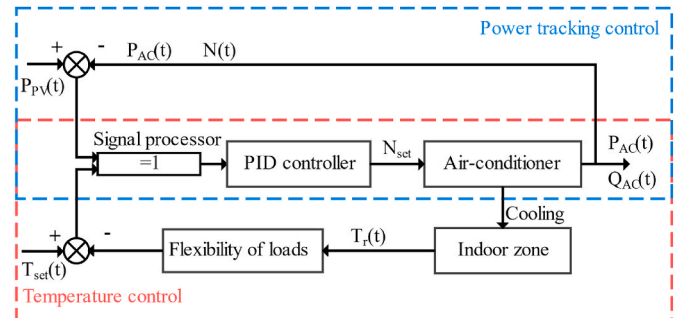


Fig. 3. Control schematic of the power matching and the indoor temperature.

air conditioning operation based on the temperature setpoint (T_{set}). Conventional variable-frequency air conditioners can be regarded as controlling the air conditioning operation based on the difference between T_{set} and $T_r(t)$. However, in this study, an additional judgment is made based on the flexibility of cooling loads. The specific control strategies will be mentioned later in the text.

It is important to note that the two control loops do not simultaneously affect the air conditioning operation. In the signal processor, only one of either the power tracking signal or the thermal comfort control signal is selected based on the predefined operating strategy. Therefore, only one signal will be applied to the PID controller at any given time, thus changing the air conditioning operation accordingly.

3.2. Optimization of control strategies

Different control strategies of the PVAC system can affect both the energy matching performance of the system and the indoor thermal environment. The evaluation results of these two aspects often contradict each other. When changing the control strategy to improve thermal comfort, the energy matching performance of the system is often compromised. In this study, we employed rule-based control methods, initiating with the optimal scenario for energy matching and subsequently refining control strategies to enhance thermal comfort. Three control strategies were proposed. The implementation of control strategies is illustrated in Fig. 4. The process includes three steps. The first step is to set the system parameters, including the compressor speed range (N_{min} , N_{max}), temperature setpoint (T_{set}), indoor thermal comfort temperature range (T_{min} , T_{max}), and the desired temperature range (ΔT) (which will be explained in section 3.2.3). The second step is to measure the relevant parameters in real-time during system operation, including $P_{PV}(t)$, $P_{AC}(t)$, $N(t)$, and $T_r(t)$. The third step involves calculating the controllable parameter setpoints based on real-time measurement parameters and the predefined operating strategy, followed by appropriate control actions.

It should be noted that this study centered on cooling operations during summer for the control strategies, experiments, and simulations.

3.2.1. Maximum of energy matching strategy

To explore the power response and energy matching performance of the PVAC system, a maximum energy matching control strategy (ST_E) was proposed as shown in Fig. 5. The principle behind control strategy is

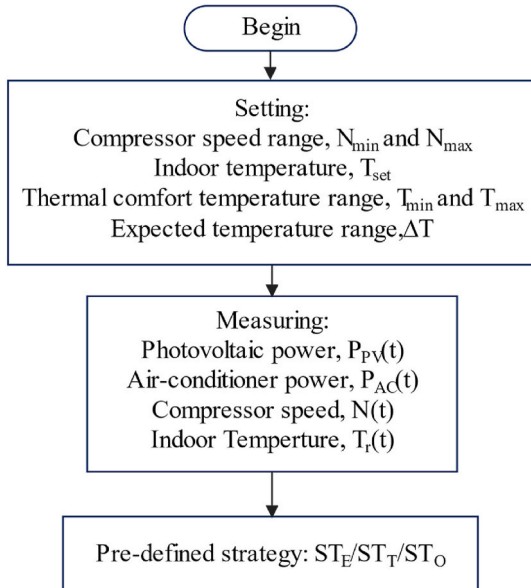


Fig. 4. Operation control of the PVAC system.

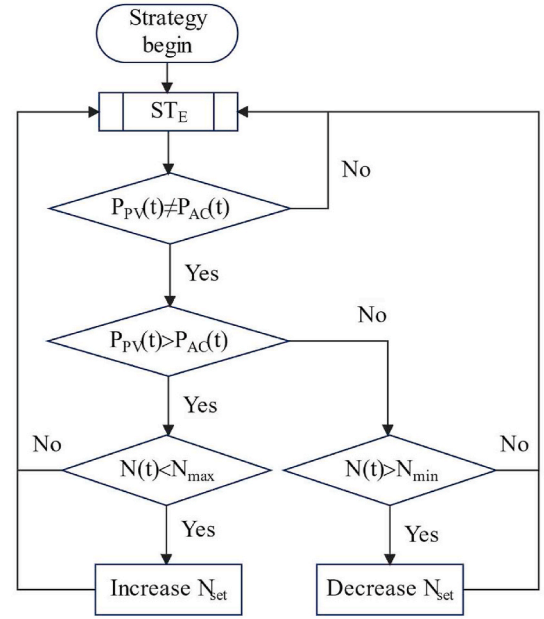


Fig. 5. The maximum of energy matching strategy.

to make the air conditioning power consumption as close as possible to the PV power generation. When $P_{PV}(t)$ and $P_{AC}(t)$ are detected to be unequal, the control strategy calculates a new compressor speed setpoint using the PID controller based on the magnitude and difference between the PV power supply and AC power demand, within the predetermined compressor speed range. The control instruction is then sent to the speed controller to adjust the air conditioning power demand.

This control strategy effectively increases the self-consumption rate and the self-sufficiency rate of the PVAC system. However, it does not consider the control of indoor temperature, which may lead to the overheating or overcooling of the indoor environment. Therefore, the feasibility of this strategy is limited in terms of practical applications.

3.2.2. Thermal comfort temperature control strategy

For the indoor thermal comfort environment design of residential buildings, a common approach is to build a thermally neutral environment to ensure the thermal satisfaction of the majority of occupants. The primary factor influencing occupants' thermal comfort in the indoor environment is temperature, and there is an acceptable temperature range known as the thermal comfort temperature range (TCTR). In this study, the TCTR for summer conditions is considered to be 23.9 °C–28.3 °C [40]. Therefore, a thermal comfort temperature control strategy (ST_T) was proposed, as shown in Fig. 6.

First, the real-time indoor temperature ($T_r(t)$) is checked to see if it falls within the TCTR. If it falls within the range, the PVAC system is controlled using the ST_E strategy to maximize the energy matching. If $T_r(t)$ is outside of the TCTR, its position relative to the range is determined. When $T_r(t)$ is less than or equal to the lower limit of the TCTR (T_{min}), the indoor temperature setpoint (T_{set}) is set to T_{min} . In this case, the PV generation may exceed the air conditioning demand, and the excess PV generation will be fed into the utility grid. The ST_E strategy is then applied to control the PVAC system when $T_r(t)$ is back within the TCTR. Similarly, when $T_r(t)$ is greater than or equal to the upper limit of the TCTR (T_{max}), T_{set} is set to T_{max} . In this case, the PV generation may be insufficient to meet the air conditioning power demand, and the utility grid supplements the shortage of PV generation. After that, the ST_E strategy is applied to control the PVAC system.

The control strategy in Fig. 6 ensures that the indoor temperature remains within the TCTR during the PVAC operation, while simultaneously striving to achieve energy matching between PV power

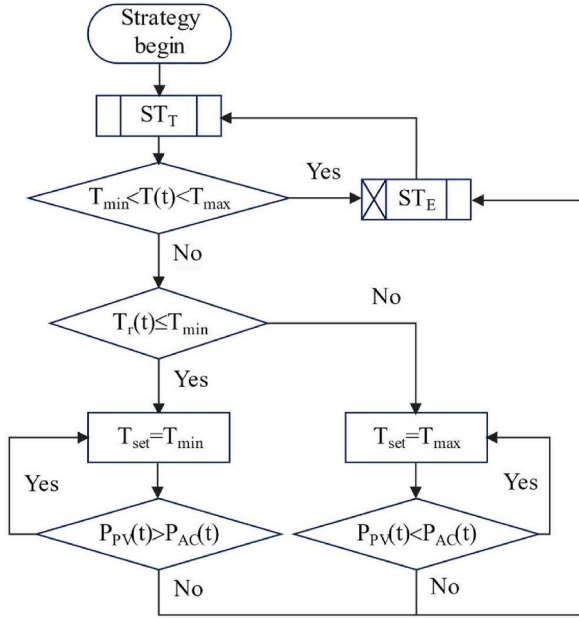


Fig. 6. The temperature control strategy.

generation and air conditioning power consumption. However, this strategy might result in the room temperature staying at the boundaries of the thermal comfort temperature range for a long time, which can affect the occupants' thermal satisfaction, especially when the PVAC system capacity is poorly designed or operating under extreme weather conditions. Therefore, further optimization is still needed.

3.2.3. Optimization of occupant thermal comfort strategy

Compared to a steady indoor temperature, occupants generally favor a fluctuating indoor environment [41]. In air-conditioned buildings, individuals are more sensitive to temperature, and their desired TCTR is narrow [42]. Based on these considerations, a control strategy called Optimization of Occupant Thermal Comfort (ST_O) was proposed, aiming

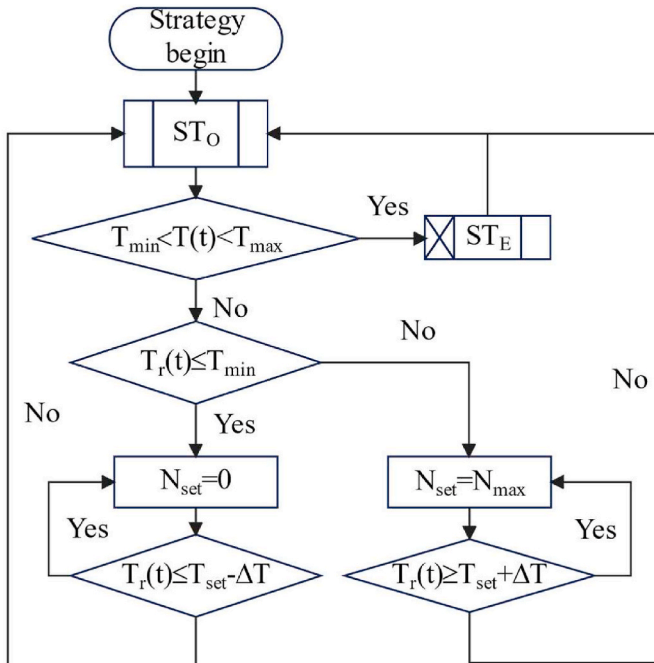


Fig. 7. Optimization strategy for the building occupant thermal comfort.

to improve the thermal comfort for the occupants. The control flowchart is shown in Fig. 7.

In this strategy, T_{set} is set to 26 °C, and the desired temperature range (ΔT) is set to ± 1 °C away from T_{set} . First, similar to the ST_T strategy, $T_r(t)$ is checked to see if it falls within the TCTR. If it falls within the range, the PVAC system is controlled using the ST_E strategy. If it is outside the range, the temperature range is considered. When $T_r(t)$ is less than or equal to T_{min} , the air conditioning is switched off ($N_{set} = 0$) until the indoor temperature rises to the lower limit of the desired temperature range (i.e., $T_r(t) = T_{set} - \Delta T$). The process then goes back to the first step. When $T_r(t)$ is greater than or equal to T_{max} , the air conditioning operates at the maximum capacity ($N_{set} = N_{max}$) until the indoor temperature decreases to the upper limit of the desired temperature range (i.e., $T_r(t) = T_{set} + \Delta T$). The process then goes back to the first step.

Compared to the maximum energy matching control strategy (ST_E) and the thermal comfort temperature control strategy (ST_T), ST_O narrows down the desired temperature range and avoids the system staying at the boundaries of the TCTR for prolonged periods of time. It ensures a variable indoor thermal environment while maintaining a good level of thermal comfort for the occupants. This strategy has practical feasibility. Additionally, it should be noted that T_{set} and ΔT are used as an example in this study and can be adjusted according to the actual situation. The performance of the system may vary with different parameter settings.

4. Experiments and model validation

4.1. Experimental method

The PVAC system was devised and set up at the Lab of Building Energy with Smart Technologies (BEST) located at Hunan University (28.17° N , 112.95° E). The system schematic is shown in Fig. 8. The size of the experimental room is 8m × 2.2m × 3m. Six PV panels with a rated power capacity of 410 W were installed outside. The PV panels, the utility grid and the energy-using side were connected to an inverter, through which the energy flow and the power balance were controlled. The energy-using side includes an air conditioner with a rated power of 1.3 kW and a control box. The specifications and characteristics of the main components are shown in Table 1. The control box compiles collected signals, which encompass data from the inverter, sensors, and air conditioner, and then transmits them to the upper control platform (UCP). The control strategy was programmed in Java and then UCP calculates the operating state and sends them to the control box, which subsequently controls the operation of the air conditioner.

To maximize the energy matching performance of the PVAC system, the slope limit of the air conditioning compressor speed was set to the maximum recommended value of 40 rpm/s. Before initiating the experiments, we equipped the PVAC system with sensors to gauge a variety of operational parameters. Three pyranometers were used to measure direct solar radiation (MS57), diffuse solar radiation (MS80A), and the total horizontal solar radiation (MS80A). Temperature and humidity sensors were placed outside the building to measure the outdoor environmental conditions. Three temperature and humidity sensors were uniformly distributed at a height of 1.5 m inside the building to measure the average indoor temperature and humidity. Three power meters were installed on the PV side, air conditioner side, and the utility grid side, each of which was able to measure the power and voltage data. All the external sensors and air conditioning communication lines were connected to a Direct Data Controller (DDC), which was then connected to the upper control platform via Ethernet TCP. The time interval for data collection and control was set to 1 s. The characteristics of the instruments are shown in Table 2.

The experiments took place from August to October 2022, and they were segmented into three distinct stages. In the first stage, a continuous five-day operation test was conducted without changing the control strategy of the air conditioning system (i.e., following the conventional variable frequency control method with $T_{set} = 26$ °C) to establish a

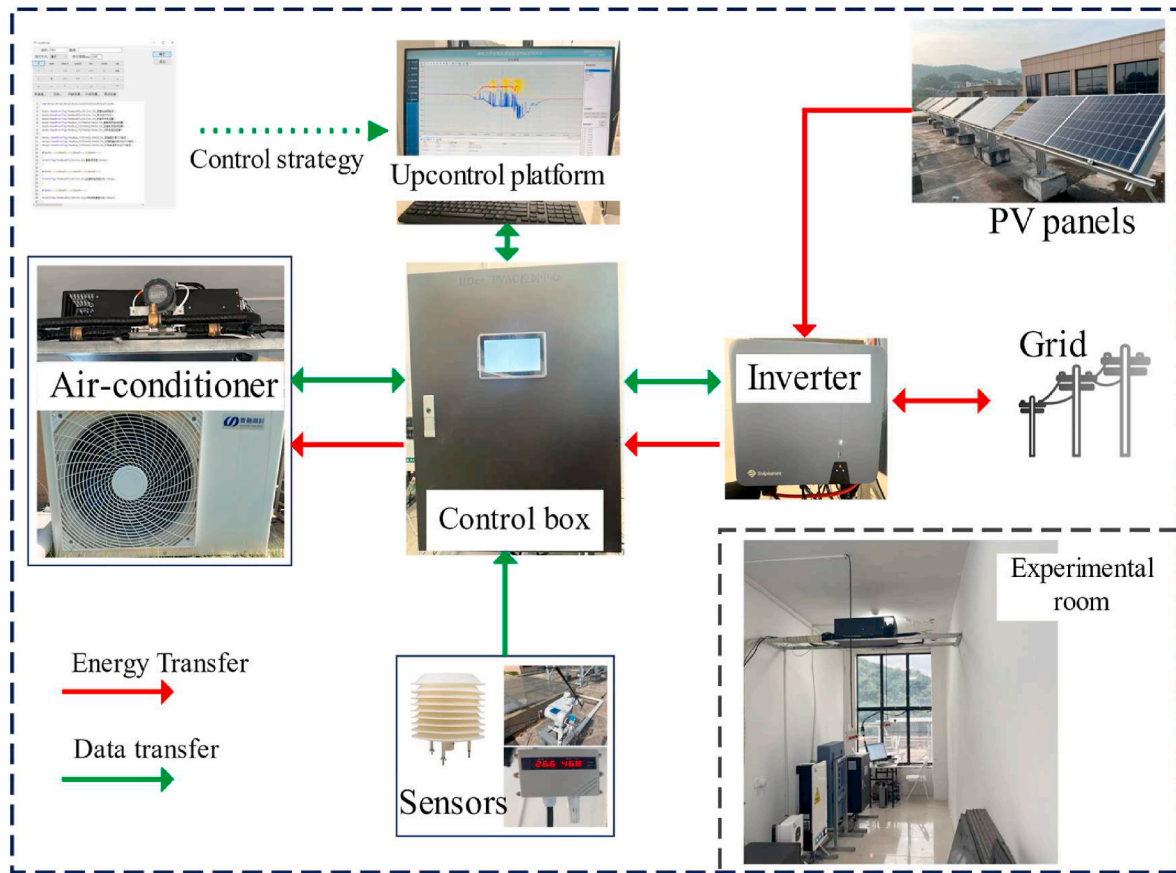


Fig. 8. Schematic diagram of the PVAC system.

Table 1

Specifications of the devices in the PVAC system.

| Component | Specifications and characteristics |
|-----------------|---|
| PV panel | TSM-410 N,Pmax: 410 W \pm 3 % , Vmp:42.6 V, Imp: 9.63 A, Voc:50.0 V \pm 3 % , Isc:10.25 A \pm 5 % |
| Inverter | Max PV power:5000 W, Mpp voltage range:40–530 V |
| Air-conditioner | Rated input:1.3 kW, Compressor speed:1200–3000 rpm |

Table 2

Characteristics of the instruments used in the experiments.

| Devices | Model | Range | Accuracy |
|---------------------------------|---------------|-------------------------|----------|
| Pyranometer | MS57 | 0–1600 W/m ² | 0.2 % |
| | MS80A | 0–1600 W/m ² | 0.2 % |
| Temperature and humidity sensor | Model41382 VC | –20–60 °C | 0.5 °C |
| | | 0%–100%RH | 3%RH |
| Electricity meters | DTST1352 | 0–380 V | 0.2 % |
| | | 0–10(100)A | 0.2 % |
| Direct Data Controller | S7-1200 | 0–20 mA | 0.5 % |
| | | 0–10 V | 0.5 % |

baseline strategy (ST_B). In the second stage, the proposed maximum energy matching strategy (ST_E) was implemented for five continuous days of operation, and the accuracy of the model was validated based on the data obtained from this stage. In the third stage, the thermal comfort temperature control strategy (ST_T) and the optimization of occupant thermal comfort strategy (ST_O) were tested for a full day to evaluate the system performance and the feasibility of the strategies. To avoid the influence of the initial indoor temperature on the experiment results, the PVAC system was operated for two days using the strategy before carrying out the experiments.

4.2. Model validation

The emphasis of model validation was primarily on the PV power generation and variations in indoor temperature. PV power generation is the main energy source for the PVAC system and plays a decisive role during the system's operational state in most cases. Meanwhile, the variation of indoor temperature during system operation is of great concern to the building occupants. To assess the simulation model's accuracy, we utilized the root mean square error (RMSE), as depicted in Eq. (14):

$$RMSE = \sqrt{\frac{1}{n} \sum_{i=1}^n (x_i - x'_i)^2} \quad (14)$$

In Equation (14), x_i and x'_i represent the experiment data and the simulation results, respectively.

A simulation model was built using Python. The model was validated using the experimental results with the ST_E strategy and the weather

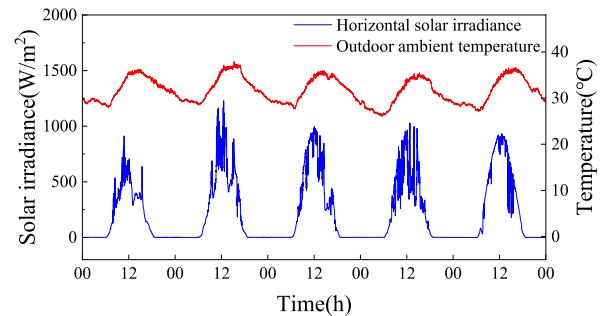


Fig. 9. Weather data in model validation.

data are shown in Fig. 9. Fig. 10 shows the experiment data and simulation results for the ST_E strategy case. The simulation results match the experimental data well, no matter whether it is a sunny or cloudy day. For the PV power generation model, as shown in Fig. 10(a), the average relative error between the experiment and simulation data was 5.94 %, and the RMSE was 33.19 W. Regarding the indoor temperature variation, as shown in Fig. 10(b), the simulated results closely match the measured data in terms of trend, with a small deviation, and the RMSE was 0.54 °C.

4.3. Feasibility analysis of various strategies

The four different control strategies of the PVAC system, namely ST_B, ST_E, ST_T and ST_O, were implemented and evaluated through the experiments. The daily performance of the strategies is shown in Fig. 11. It should be noted that due to the inherent variability of weather conditions, it was challenging to replicate identical conditions for each experiment to test the different strategies. However, we made efforts to select days with similar ambient temperatures for the experiments to ensure a reasonable level of comparability. Despite these efforts, solar radiation levels varied due to factors such as cloud cover, which were beyond our control. As a result, each experiment was conducted under conditions that were as close as possible, but not identical.

In this study, due to the presence of a large west-facing exterior wall in the experimental room, the cooling load in the afternoon was significantly higher than that in the morning. Fig. 11(a) shows the performance of the ST_B strategy. After the PVAC system was initiated, the indoor temperature rapidly approached the set temperature T_{set} (26 °C) due to the cooling effect of the air conditioning. During this process, the main factor affecting the air conditioning power was the difference between T_r and T_{set} . When the cooling load was too low, as shown at 08:14, the indoor temperature dropped below 25 °C, and the air conditioning stopped running until the temperature reached 26.6 °C (08:52), at that point the air conditioning operated again. During the working period, the air conditioning was able to maintain the indoor temperature near the set temperature. However, when the cooling load varied significantly, such as when the room experienced a rapid increase of cooling load due to the direct sunlight heat gain in the afternoon or a rapid decrease of cooling load as the sun set, the effectiveness of the temperature control decreased. This is related to the thermal inertia of the room and the uneven distribution of air temperature. Overall, there is potential for significant optimization in terms of cooling demand and PV generation alignment, considering the load flexibility of the air conditioning.

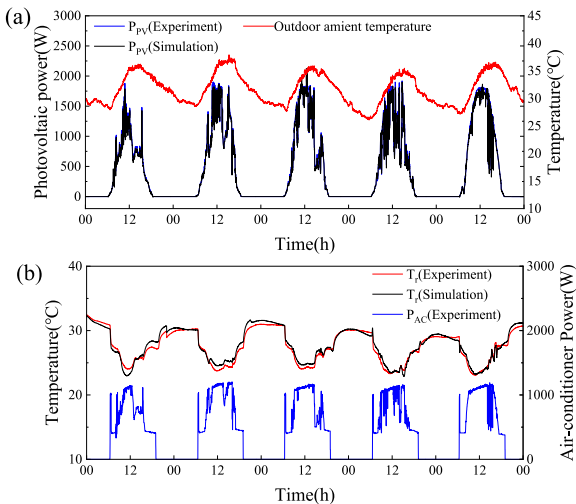


Fig. 10. Comparison between the experiment data and simulation results.

Fig. 11(b) shows the results of the ST_E strategy. The PV power generation and the air conditioning power consumption are strongly correlated within the operating capacity of the air conditioner. However, since the room temperature was not considered, it often resulted in prolonged periods of overcooling during the experiments, as seen during the daytime. The ST_T strategy addresses this overcooling issue, as shown in Fig. 11(c). When the temperature reached T_{max} (28.3 °C) at 17:03, the temperature was maintained at that value by changing the T_{set} to T_{max} . As the PV generation was consistently lower than the air conditioning power demand, this setting remained unchanged, but the deficiency in power supply is filled by the utility grid. The ST_H strategy further optimizes the control based on the ST_T strategy, as shown in Fig. 11(d). On the experimental day, when the temperature reached T_{min} (23.9 °C), the air conditioning was turned off and PV power was uploaded to the utility grid until the temperature increased to the lower limit of the desired temperature range ($T_{set} - \Delta T = 25$ °C), at that point the air conditioning restarted. Similarly, when the temperature reached T_{max} (28.3 °C), the air conditioning operates at the maximum capacity and the utility grid replenish the shortage of PV power until the temperature dropped to the upper limit of the desired temperature range ($T_{set} + \Delta T = 27$ °C), after which the system continued operating according to the ST_E strategy. The outcomes from the operations resonate with the predictions and analyses from Section 3.2, underscoring the practical viability of the optimization strategies.

5. Results and discussion

5.1. Power tracking performance

Improving the power tracking capability is pivotal to optimize the energy matching performance for PVAC systems. After consulting the air conditioning manufacturer in this study, we configured the compressor to operate at its peak ramp rate during the experiments to analyze its interactions with the PVAC system and the utility grid, as shown in Fig. 12. Fig. 12(a) illustrates the variations of $P_{PV}(t)$, $P_{AC}(t)$, horizontal solar irradiance ($G_h(t)$), and compressor speed ($N(t)$) during a certain period of the experiment, while Fig. 12(b) provides the variation of the grid power ($P_{Grid}(t)$) and the voltage ($V_{Grid}(t)$) at the utility grid connection point during the same time period.

Initially, the air conditioning system operated at the maximum capacity, with the compressor speed ($N(t)$) reaching its maximum value (N_{max}), PV power generation exceeded the air conditioning power demand, and the surplus electrical energy was uploaded into the utility grid, leading to negative values of $P_{Grid}(t)$. When $P_{PV}(t)$ is suddenly decreased due to solar radiation variations and is lower than the air conditioning power demand $P_{AC}(t)$, the shortfall in electrical energy is supplied by the utility grid, which results in a sudden change of $P_{Grid}(t)$ and a corresponding drop of $V_{Grid}(t)$. Subsequently, through PID control, the compressor speed is reduced, leading to a decrease in $P_{AC}(t)$ and a gradual reduction of $P_{Grid}(t)$ to zero, along with a rebound in $V_{Grid}(t)$. Similarly, when $P_{PV}(t)$ is suddenly increased, $P_{AC}(t)$ gradually increases, and the excess electrical energy is fed back to the utility grid, causing $P_{Grid}(t)$ to decrease abruptly and then gradually rebound. The same effect is observed in $V_{Grid}(t)$.

Fig. 13 presents the testing results to assess the power response capabilities under the conventional air conditioning control strategy, referred to the baseline strategy (ST_B). When T_{set} changed, $P_{AC}(t)$ started to vary accordingly. In our experiments, when T_{set} was changed by 1 °C and 2 °C, the corresponding changes of $P_{AC}(t)$ were 0.077 kW and 0.282 kW, with time intervals of 2.5 min and 5 min, respectively. However, in the case shown in Fig. 12 under the ST_E strategy, when $P_{AC}(t)$ changed by 0.70 kW (close to the maximum range of the air conditioning power regulation), it only took 1.1 min. By exerting direct control over the compressor to change the air conditioning operating status, the power response speed of air conditioning was significantly improved.

In this study, we achieved power tracking control within a few

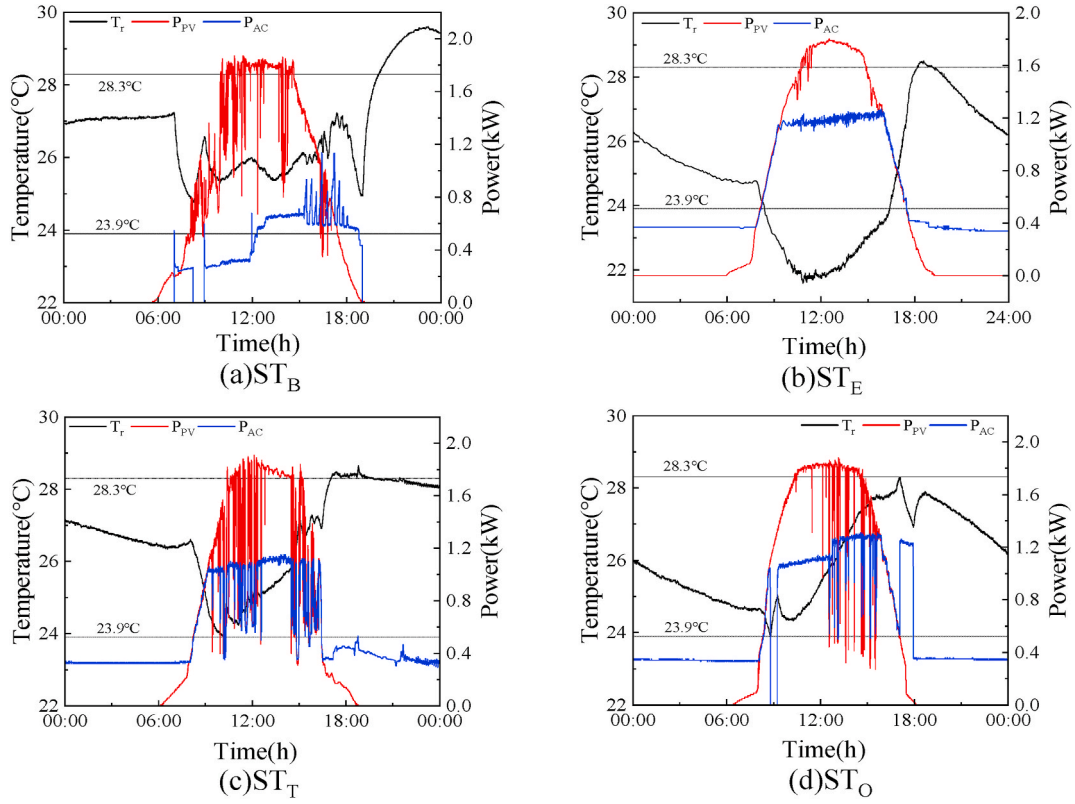


Fig. 11. The operation performance of the different strategies of the PVAC system.

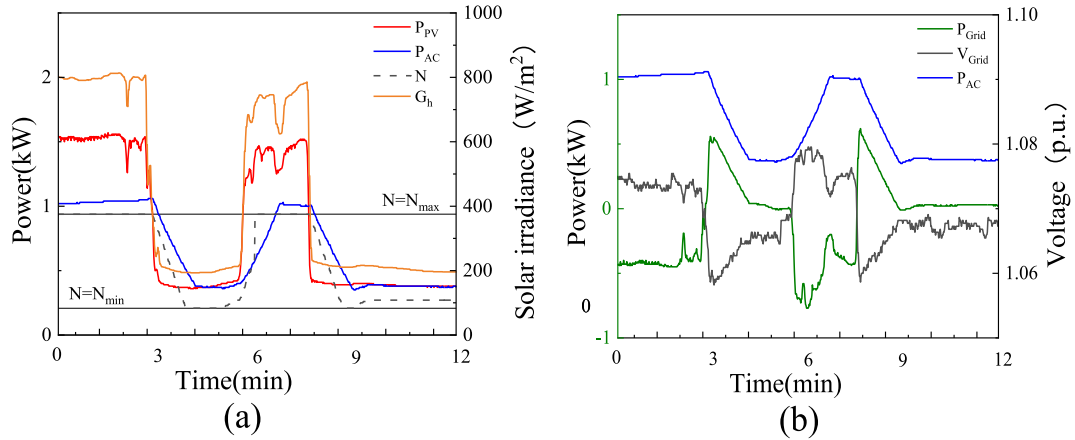


Fig. 12. PVAC System performance under the power tracking control.

seconds or tens of seconds, demonstrating the capacity for sub-minute power tracking. This rapid response is crucial for real-time zero-energy consumption in PVAC systems and enhances the stability of the utility grid's net power and voltage. Similarly, reference [19] explores the benefits of dynamically adjusting compressor speed to smooth out fluctuations in PV power generation, further validating the potential of dynamic control strategies in PV systems.

5.2. System performance

The measured meteorological data in Changsha from May 1st to October 31st, 2022, were used as inputs for simulating the PVAC's performance in cooling season. The time interval of the data collection is 1 min. Simulation results were used to analyze the performance of the PVAC system in terms of energy matching and room temperature control

throughout the cooling season.

Both SCR and SSR serve as pivotal performance metrics in assessing PVAC systems, and RZEP can assess the real-time energy matching performance of the PVAC system, as shown in Fig. 14. From the simulation results of the entire cooling season, the SCR and SSR are 0.530 and 0.716, respectively, for the baseline strategy (ST_B). The other three proposed strategies significantly improved these evaluation results, with the increases in SCR and SSR being notably higher than those achieved by simply adjusting the setpoint temperature for energy matching [22]. Among the three strategies, the maximum energy matching control strategy (ST_E) maximizes the consumption of PV power generation and minimizes the demand from utility grid, which results in a higher SCR and SSR values of 0.774 and 0.869, respectively. The thermal comfort temperature control strategy (ST_T) and the optimization of occupant thermal comfort strategy (ST_O) sacrifice a little bit of energy matching

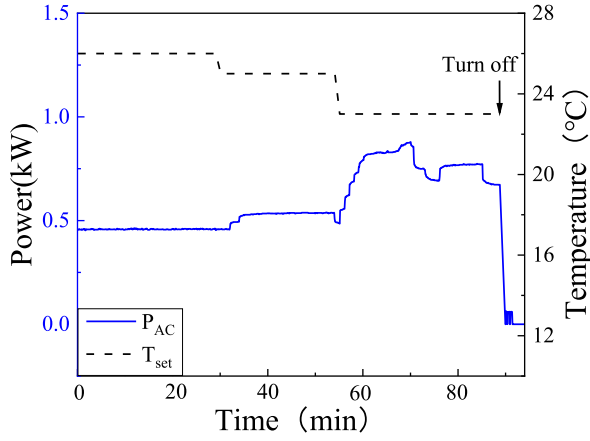


Fig. 13. Power response in temperature control mode (Baseline strategy).

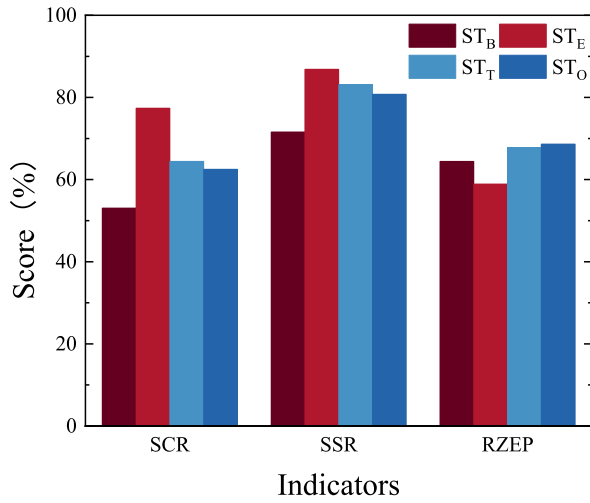


Fig. 14. Scores of the evaluation indicators for different strategies.

performance to ensure the thermal comfort in the indoor environment. For the system's RZEP, the ST_E strategy performed the worst with a value of 0.589 for RZEP, while the ST_O strategy performed the best with a value of 0.687 for RZEP. The subpar performance of the ST_E strategy is due to the fact that the primary concern in evaluating zero-energy consumption of the PVAC system is to meet the occupants' demand of indoor comfort. Conversely, the ST_T strategy's performance is attributed to maintaining the temperature at the boundary of the TCTR when it reaches this boundary creates more non-real-time zero energy potential compared to the ST_O strategy. In this study, whether the indoor temperature is within the TCTR is taken as a prerequisite for evaluating zero-energy consumption. With the ST_E strategy, there were periods during which the indoor temperature was outside of the thermal comfort range for a relatively long period of time, resulting in poor RZEP performance. On the other hand, the ST_O strategy aimed to keep the temperature within the TCTR, and when the temperature reached the upper or lower boundary of the TCTR, the system responded by either stopping or operating the air conditioning system at the maximum capacity until the temperature returned to the desired range. The operating results indicate that the performance of the optimization strategies in practical operation aligns with the results expected and analyzed in Section 3.2, thereby demonstrating the feasibility of the proposed control strategies.

In addition to the energy performance, the ability of different strategies to control the indoor temperature was also evaluated. Fig. 15 contrasts the indoor temperature ranges under various control strategies during the PVAC system's operation. It is seen that the ST_B strategy,

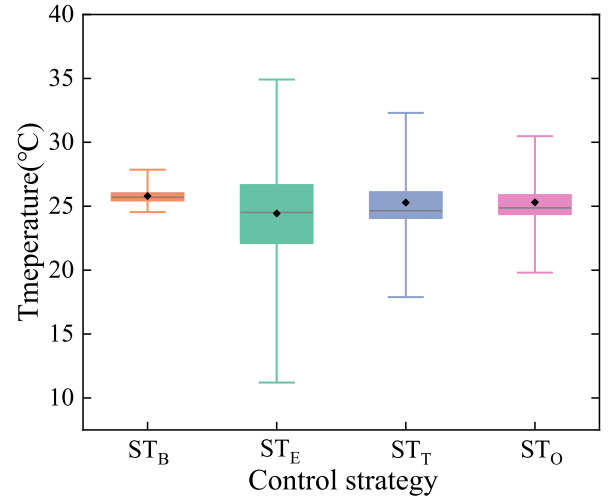


Fig. 15. Room temperature range during operation of the PVAC system.

which relies on temperature as the control signal input, exhibits the best control on the indoor temperature, consistently maintaining it near T_{set} (26 °C). The Mean Absolute Error (MAE) of temperature values for the temperature control under different control strategies are presented in Table 3. It is shown that the ST_E strategy has the weakest temperature control performance and is only suitable for specific cooling demand scenarios. The ST_T strategy demonstrates a relatively good temperature control performance and can satisfy the thermal comfort requirements in most cases. The ST_O strategy has the most adjustable parameters for temperature control, allowing it to adapt to different scenarios or residents' needs. Due to its good temperature control performance and energy matching performance, the ST_O strategy is recommended in this study.

5.3. Energy storage capacity analysis

Energy storage, particularly through batteries, is often incorporated with PV systems to mitigate the variability of PV power generation and enhance energy matching performance. The battery is modeled based on the state of charge (SOC), as shown in Eq. (15):

$$SOC|_{t+1} = SOC|_t + \eta_{ch} \frac{P_{b,ch}(t) \times \tau}{E_b} - \frac{P_{b,dis}(t) \times \tau}{\eta_{dis} \times E_b} \quad (15)$$

In Equation (15), $P_{b,ch}(t)$ and $P_{b,dis}(t)$ represent the charging and discharging power of battery, respectively, and η_{ch} and η_{dis} represent the charging and discharging efficiencies of the battery, respectively. E_b represents the battery capacity, and τ represents the time step.

Lithium batteries were used in this study, plays a crucial role in managing PV surpluses. Embracing the principle of 'self-generation and self-consumption of PV power,' the control strategies ensure that any PV surpluses are primarily directed to these batteries. The aim is to store this surplus energy for later use, ensuring an efficient energy matching. When the PV panels produce surplus electricity, it is first channeled to charge the batteries. Only when the batteries reach their optimal capacity, the excess energy is regulated and managed by the utility grid. This control mechanism not only prioritizes the efficient use of self-generated PV power but also optimizes the utilization of the energy storage capacity of the batteries.

As shown in Fig. 16, this study further analyzed the energy matching

Table 3
MAE comparison between different control strategies.

| Strategy | ST_B | ST_E | ST_T | ST_O |
|----------|--------|--------|--------|--------|
| MAE | 0.553 | 2.977 | 1.569 | 1.295 |

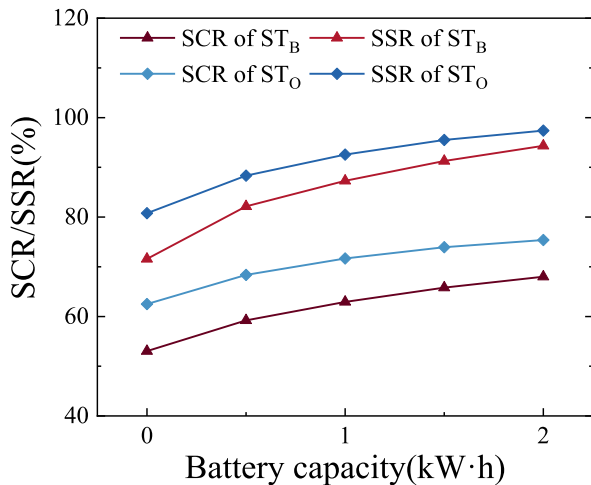


Fig. 16. Energy performance of the PVAC system with different battery capacities.

performance of the proposed ST_O strategy and the baseline strategy (ST_B) under different energy storage capacities. With the increase in battery capacity, both the SCR and SSR gradually improve. This improvement is attributed to the prioritization of battery storage for managing any mismatch between PV generation and air conditioning consumption. By utilizing the batteries to absorb excess PV power or to compensate for any shortfall, a higher proportion of self-generated PV energy is used directly by the system, thereby enhancing the SCR and SSR. Additionally, the SSR value consistently exceeds the SCR value, indicating that the PV system was designed with a capacity surplus, where the total PV power generation during the entire cooling season surpasses the total energy consumption of the air conditioning system.

Comparing the proposed ST_O strategy with the ST_B strategy, the ST_O strategy achieved an SCR of 0.625 and an SSR of 0.808 without any battery capacity. Meanwhile the ST_B strategy required a 1 kWh battery capacity to achieve similar values, resulting in an SCR of 0.629 and an SSR of 0.873. This demonstrates that the proposed method can reduce the need of energy storage in the system, which would reduce the initial investment costs of the system.

Overall, the results and discussion demonstrate the effectiveness of the proposed strategies in improving the energy matching performance, power tracking capabilities, and temperature control performance of PVAC systems.

6. Conclusions

This study proposed a novel PV direct-driven air conditioning (PVAC) system designed to dynamically track real-time PV power generation by directly adjusting the air conditioner's compressor speed. Three control strategies were developed, experimentally validated, and simulated throughout the cooling season. Evaluation metrics such as self-consumption ratio (SCR), self-sufficiency ratio (SSR), real-time zero-energy performance (RZEP), and mean absolute error (MAE) of temperature were utilized to compare the different control strategies in terms of energy matching performance and ability to achieve the indoor thermal comfort. Furthermore, the energy performance of the baseline strategy (ST_B) and optimization of occupant thermal comfort strategy (ST_O) under different battery capacities was discussed. Key conclusions are outlined as follows:

- (1) The study proposed an innovative control method that regulates the speed of the air conditioning compressor according to the PV power generation. This method allows power tracking with sub-

minute power response and significantly mitigates the impact of the PV power fluctuations on utility grid.

- (2) The control strategies proposed were successfully implemented, showcasing commendable performance in terms of energy efficiency and occupant thermal comfort during experiments. Considering the indoor temperature control effect and the energy matching performance of the PVAC system, the ST_O strategy emerged as the preferred strategy.
- (3) The ST_O strategy improved the SCR from 0.53 to 0.625 and the SSR from 0.716 to 0.808 compared to the baseline strategy (ST_B), demonstrating significant advancements in real-time energy matching.
- (4) The proposed control strategies reduced the need for energy storage, thereby lowering the initial investment and operational costs of the PVAC system.

The proposed power control methods and strategies add minimal complexity to the system and are adaptable across diverse scenarios. Future research should focus on optimizing battery capacity to maximize PV consumption and exploring strategies to enhance overall system performance.

CRediT authorship contribution statement

Kai Wang: Formal analysis, Investigation, Methodology, Validation, Writing – original draft. **Jinqing Peng:** Writing – review & editing, Conceptualization, Methodology, Supervision. **Sihui Li:** Investigation, Writing – review & editing. **Houpei Li:** Writing – review & editing, Validation. **Bin Zou:** Investigation, Supervision. **Tao Ma:** Writing – review & editing. **Jie Ji:** Writing – review & editing.

Declaration of competing interest

The authors declare that they have no known competing financial interests or personal relationships that could have appeared to influence the work reported in this paper.

Data availability

Data will be made available on request.

Acknowledgements

This study was sponsored by the National Key R&D Program of China (2022YFB4201003), the National Natural Science Foundation of China (No.52278104), the Natural Science Foundation of Hunan Province (2021JJ40107) and the science and technology innovation Program of Hunan Province (No. 2023RC1042).

References

- [1] International Energy Agency. *World energy outlook*. 2022.
- [2] Lin J, Liu Xu, He Gang. Regional electricity demand and economic transition in China. *Util Pol* 2020;64. <https://doi.org/10.1016/j.jup.2020.101047>.
- [3] Izam NSMN, Itam Z, Sing WL, Syamsir A. Sustainable development perspectives of solar energy technologies with focus on solar photovoltaic—a review. *Energies* 2022;15. <https://doi.org/10.3390/en15082790>.
- [4] Karimi M, Mokhlis H, Naidu K, Uddin S, Bakar AHA. Photovoltaic penetration issues and impacts in distribution network - a review. *Renew Sustain Energy Rev* 2016;53:594–605. <https://doi.org/10.1016/j.rser.2015.08.042>.
- [5] Guo YY. Revisiting the building energy consumption in China: insights from a large-scale national survey. *Energy for Sustainable Development* 2022;68:76–93. <https://doi.org/10.1016/j.esd.2022.03.005>.
- [6] Ahmed A, Ge T, Peng J, Yan WC, Tee BT, You S. Assessment of the renewable energy generation towards net-zero energy buildings: a review. *Energy Build* 2022; 256. <https://doi.org/10.1016/j.enbuild.2021.111755>.
- [7] Chaudhary P, Rizwan M. Voltage regulation mitigation techniques in distribution system with high PV penetration: a review. *Renew Sustain Energy Rev* 2018;82: 3279–87. <https://doi.org/10.1016/j.rser.2017.10.017>.

- [8] Overgeneration from solar energy in California. A field guide to the duck chart. Golden, CO (United States): National Renewable Energy Lab. (NREL); 2015. Technical report.
- [9] Liang G, Sun B, Zeng Y, Ge L, Li Y, Wang Y. An optimal allocation method of distributed PV and energy storage considering moderate curtailment measure. *Energies* 2022;15. <https://doi.org/10.3390/en15207690>.
- [10] Li S, Peng J, Tan Y, Ma T, Li X, Hao B. Study of the application potential of photovoltaic direct-driven air conditioners in different climate zones. *Energy Build* 2020;226. <https://doi.org/10.1016/j.enbuild.2020.110387>.
- [11] Kim DS, Infante Ferreira CA. Solar refrigeration options - a state-of-the-art review. *Int J Refrig* 2008;31:3–15. <https://doi.org/10.1016/j.ijrefrig.2007.07.011>.
- [12] Chandel R, Chandel SS, Prasad D, Dwivedi RP. Prospects of sustainable photovoltaic powered thermoelectric cooling in zero energy buildings: a review. *Int J Energy Res* 2022;46:19319–40. <https://doi.org/10.1002/er.8508>.
- [13] Siecker J, Kusakana K, Numbi BP. A review of solar photovoltaic systems cooling technologies. *Renew Sustain Energy Rev* 2017;79:192–203. <https://doi.org/10.1016/j.rser.2017.05.053>.
- [14] Hu L, Liu Y, Wang D, Luo X, Liu H. Feasibility analysis and feature comparison of cold thermal energy storage for off-grid PV air-conditioned buildings in the tropics. *Energy Convers Manag* 2022;254. <https://doi.org/10.1016/j.enconman.2021.115176>.
- [15] Fanoro M, Božanić M, Sinha S. A review of the impact of battery degradation on energy management systems with a special emphasis on electric vehicles. *Energies* 2022;15. <https://doi.org/10.3390/en15165889>.
- [16] Li S, Peng J, Zou B, Li B, Lu C, Cao J, et al. Zero energy potential of photovoltaic direct-driven air conditioners with considering the load flexibility of air conditioners. *Appl Energy* 2021;304. <https://doi.org/10.1016/j.apenergy.2021.117821>.
- [17] Li Y, Zhao BY, Zhao ZG, Taylor RA, Wang RZ. Performance study of a grid-connected photovoltaic powered central air conditioner in the South China climate. *Renew Energy* 2018;126:1113–25. <https://doi.org/10.1016/j.renene.2017.05.064>.
- [18] Li S, Peng J, Li H, Zou B, Song J, Ma T, et al. Zero energy potential of PV direct-driven air conditioners coupled with phase change materials and load flexibility. *Renew Energy* 2022;200:419–32. <https://doi.org/10.1016/j.renene.2022.09.088>.
- [19] Jiang Z, Cai J, Moses PS. Smoothing control of solar photovoltaic generation using building thermal loads. *Appl Energy* 2020;277. <https://doi.org/10.1016/j.apenergy.2020.115523>.
- [20] Gao Y, Ji J, Han K, Zhang F. Comparative analysis on performance of PV direct-driven refrigeration system under two control methods. *Int J Refrig* 2021;127: 21–33. <https://doi.org/10.1016/j.ijrefrig.2021.03.003>.
- [21] Gao Y, Ji J, Han K, Zhang F. Experimental and numerical study of a PV/T direct-driven refrigeration/heating system. *Energy* 2021;230. <https://doi.org/10.1016/j.energy.2021.120793>.
- [22] Luo Z, Peng J, Cao J, Yin R, Zou B, Tan Y, et al. Demand flexibility of residential buildings: definitions, flexible loads, and quantification methods. *Engineering* 2022;16:123–40. <https://doi.org/10.1016/j.eng.2022.01.010>.
- [23] Schibuola L, Scarpa M, Tambani C. Demand response management by means of heat pumps controlled via real time pricing. *Energy Build* 2015;90:15–28. <https://doi.org/10.1016/j.enbuild.2014.12.047>.
- [24] Zhao BY, Zhao ZG, Li Y, Wang RZ, Taylor RA. An adaptive PID control method to improve the power tracking performance of solar photovoltaic air-conditioning systems. *Renew Sustain Energy Rev* 2019;113. <https://doi.org/10.1016/j.rser.2019.109250>.
- [25] Li G, Han Y, Li M, Luo X, Xu Y, Wang Y, et al. Study on matching characteristics of photovoltaic disturbance and refrigeration compressor in solar photovoltaic direct-drive air conditioning system. *Renew Energy* 2021;172:1145–53. <https://doi.org/10.1016/j.renene.2021.03.110>.
- [26] Li H, Li J, Li S, Peng J, Ji J, Yan J. Matching characteristics and AC performance of the photovoltaic-driven air conditioning system. *Energy* 2023;264. <https://doi.org/10.1016/j.energy.2022.126509>.
- [27] Salpakari J, Lund P. Optimal and rule-based control strategies for energy flexibility in buildings with PV. *Appl Energy* 2016;161:425–36. <https://doi.org/10.1016/j.apenergy.2015.10.036>.
- [28] Pahasa J, Potejana P, Ngamroo I. MPC-based virtual energy storage system using PV and air conditioner to emulate virtual inertia and frequency regulation of the low-inertia microgrid. *IEEE Access* 2022;10:133708–19. <https://doi.org/10.1109/ACCESS.2022.3231751>.
- [29] Mahdavi N, Braslavsky JH, Seron MM, West SR. Model predictive control of distributed air-conditioning loads to compensate fluctuations in solar power. *IEEE Trans Smart Grid* 2017;8:3055–65. <https://doi.org/10.1109/TSG.2017.2717447>.
- [30] Zou B, Peng J, Yin R, Luo Z, Song J, Ma T, et al. Energy management of the grid-connected residential photovoltaic-battery system using model predictive control coupled with dynamic programming. *Energy Build* 2023;279. <https://doi.org/10.1016/j.enbuild.2022.112712>.
- [31] Yao Y, Shekhar DK. State of the art review on model predictive control (MPC) in Heating Ventilation and Air-conditioning (HVAC) field. *Build Environ* 2021;200. <https://doi.org/10.1016/j.buildenv.2021.107952>.
- [32] Huda ASN, Zivanović R. Large-scale integration of distributed generation into distribution networks: study objectives, review of models and computational tools. *Renew Sustain Energy Rev* 2017;76:974–88. <https://doi.org/10.1016/j.rser.2017.03.069>.
- [33] EnergyPlus. Engineering reference. 2014.
- [34] Gu W, Ma T, Ahmed S, Zhang Y, Peng J. A comprehensive review and outlook of bifacial photovoltaic (bPV) technology. *Energy Convers Manag* 2020;223. <https://doi.org/10.1016/j.enconman.2020.113283>.
- [35] Chua KJ, Chou SK, Yang WM, Yan J. Achieving better energy-efficient air conditioning - a review of technologies and strategies. *Appl Energy* 2013;104: 87–104. <https://doi.org/10.1016/j.apenergy.2012.10.037>.
- [36] Department of Energy. DOE-2 reference manual. 1980.
- [37] Specification for compressor, 5RS092ZKE21, no.:SC-P-51173850-A.
- [38] Blervaque Hubert, Stabat Pascal, Filfli Sila, Schumann Mathieu, Marchio Dominique. Variable-speed air-to-air heat pump modelling approaches for building energy simulation and comparison with experimental data. *Journal of Building Performance Simulation* 2016;9(2):210–25. <https://doi.org/10.1080/19401493.2015.1030862>.
- [39] Wang W, Zhou Q, Pan C, Cao F. Energy-efficient operation of a complete Chiller-air handling unit system via model predictive control. *Appl Therm Eng* 2022;201. <https://doi.org/10.1016/j.applthermaleng.2021.117809>.
- [40] Peng P, Gong G, Mei X, Liu J, Wu F. Investigation on thermal comfort of air carrying energy radiant air-conditioning system in south-central China. *Energy Build* 2019;182:51–60. <https://doi.org/10.1016/j.enbuild.2018.10.020>.
- [41] Nikolopoulou M, Steemers K. Thermal comfort and psychological adaptation as a guide for designing urban spaces. *Energy Build* 2003;35(1):95–101.
- [42] de Dear Richard J, Schiller Brager Gail, Cooper D. Developing an adaptive model of thermal comfort and preference - final report on RP-884. *Build Eng* 1997;104(1).